TECHNICAL MEMORANDUM

472

Sensitivity of the Tropospheric Circulation to Changes in the Strength of the Stratospheric Polar Vortex

T. Jung and J. Barkmeijer[1]

Research Department

[1]KNMI, De Bilt, The Netherlands

Submitted to Monthly Weather Review

July 2005

European Centre for Medium-Range Weather Forecasts
Europäisches Zentrum für mittelfristige Wettervorhersage
Centre européen pour les prévisions météorologiques à moyen terme

Series: ECMWF Technical Memoranda

A full list of ECMWF Publications can be found on our web site under:
http://www.ecmwf.int/publications/

Contact: library@ecmwf.int

European Centre for Medium-Range Weather Forecasts
Shinfield Park, Reading, RG2 9AX, England

Abstract

The sensitivity of the wintertime tropospheric circulation to changes in the strength of the Northern Hemisphere stratospheric polar vortex is studied using one of the latest verisons of the ECMWF model. Three sets of experiments were carried out: one control integration, and two integrations in which the strength of the stratospheric polar vortex has been gradually reduced and increased, respectively, during the course of the integration. The strength of the polar vortex is changed by applying a forcing to the model tendencies in the stratosphere only. The forcing has been obtained using the adjoint technique.

It is shown that, in the ECMWF model, changes in the strength of the polar vortex in the middle and lower stratosphere have a significant and slightly delayed (on the order of days) impact on the tropospheric circulation. The tropospheric response shows some resemblance to the North Atlantic Oscillation (NAO), though the centres of action are slightly shifted towards the east compared to those of the NAO. The tropospheric response over the North Pacific and North America is rather small. Furthermore, a separate comparison of the response to a weak and strong vortex forcing suggests that to first order the tropospheric response is linear. From the results presented, it is argued that particularly extended-range forecasts in the European area benefit from the stratosphere-troposphere link.

1 Introduction

The possibility of an influence of the wintertime stratospheric polar vortex on the tropospheric circulation has been a topic of increasing interest in recent years. This is because such a link, if existent, implies some predictability of the atmospheric circulation well into the extended-range (from about 10 days to one season). The reasoning is based on the observation that the stratospheric polar vortex varies relatively slowly compared to the tropospheric circulation (Baldwin et al., 2003). As a consequence, if the stratospheri c polar vortex is, for example, anomalously strong, then its temporal persistence suggests that it is likely to remain strong for some time into the near future. Therefore, if the polar vortex would have a significant impact on the tropospheric circulation, then this would increase the memory of the troposphere leaving it potentially more predictable.

The possibility of an influence of the stratospheric polar vortex on the troposheric circulation during wintertime is of considerable interest to operational forecasting centres. This is particularly true for ECMWF, where monthly ensemble forecasts with a coupled atmosphere-ocean model are routinely being carried out once a week since autumn 2004 (Vitart, 2004); and it is monthly forecasting, which is likely to benefit the most from a possible stratosphere-troposphere coupling.

The recent increase of interest in stratosphere-troposphere coupling has largely been fueled by two observervational studies (Baldwin and Dunkerton, 2001a,b). Baldwin and Dunkerton showed that stratospheric anomalies of the Arctic Oscillation (AO, Thompson and Wallace, 1998), which reflect changes in the stratospheric polar vortex, appear to "propagate" downwards into the troposphere, thereby changing the strength of the mid-latitude westerly winds as well as the strength and location of the storm tracks.

The predictive skill associated with the downward "propagation" has been estimated byCharlton et al. (2003) and Baldwin et al. (2003) using statistical models. Both studies conclude that the stratosphere-troposphere link provides some extra-skill in statistically forecasting Northern Hemisphere weather.

The stratosphere-troposphere link has also been investigated using numerical models of the atmosphere. The first such study was carried out by Boville (1984) in an attempt to quantify the impact of inaccuracies in stratospheric simulations on the model climate in the troposhere. The "inaccuracy" in the stratosphere was generated by changing the stratospheric diffusion. Boville found significant tropospheric changes compared to a control integration, the response which has a close resemblence with the spatial structure of the NAO. Similar studies have been carried out more recently by Polvani and Kushner (2002) and Norton (2003), basically confirming

the original results by Boville.

In each of the modeling studies described above the stratospheric circulation has been altered by changing the model formulation. Charlton et al. (2004) have pointed a potential shorthcoming of this approach, namely that changes in model formulation may lead to an unrealistic stratospheric climate compared to that of the control integration. Moreover, Charlton et al. highlighted that only the time mean response has been studied although it is the transient response, which is more closely related to the forecasting problem. In order to circumvent the above mentioned problems, Charlton et al. (2004) decided to study the influence of changes of the initial conditions (see also Kodera et al., 1991) in the stratosphere in the ECMWF model leaving the model unchanged. As in the other modeling studies described above, Charlton et al. (2004) found a significant tropospheric response resembling the NAO. In order to achieve this response, however, they had to introduce substantial changes to the initial conditions. Moreover, even the relatively large number of integrations considered—ensemble integrations encompassing 50 members were diagnosed—does not erradicate the fact that only three cases were considered.

In this study we revisit the stratosphere-troposphere link by means of numerical experimentation using one of the most sophisticated atmospheric circulation models, that is, the ECMWF model used operationally in 2004. As in Charlton et al. (2004), we focus on the transient response of the troposphere to perturbations of the stratospheric polar vortex in order to address the predictability problem. However, instead of of introducing a rather drastic change to the initial conditions, we efficiently perturb the model equations in the stratosphere only leaving the initial conditions and model dynamics unchanged. The forcing applied is based on the adjoint technique. Moreover, the relatively large sample size (60 forty-day integrations) ensures that reliable conlusions can be drawn. Finally, a novelty of the present study is that strong and weak polar vortex cases are considered separately in order to test the linearity of the tropospheric response.

The paper is organized as follows. In the following section the ECMWF model used in this study is briefly described. Moreover, the method used to construct the forcing, which is used to change the stratospheric polar vortex, is outlined. The results are given in Section 3, which includes diagnosis of the zonally averaged zonal mean wind response as well as changes of the horizontal circulation at three pressure levels (50, 500 and 1000hPa). Moreover, the response of the tropospheric transient eddies is studied. Finally, the main findings of this study will be discussed

2 Methods

In order to study the sensitivity of the tropospheric circulation to changes in the strength of the polar vortex three sets of numerical experiments were carried out:

$$d\mathbf{x}^i/dt = G(\mathbf{x}^i), \quad (1)$$

$$d\mathbf{x}^i/dt = G(\mathbf{x}^i) + \mathbf{F}, \quad (2)$$

$$d\mathbf{x}^i/dt = G(\mathbf{x}^i) - \mathbf{F}, \quad (3)$$

where $\mathbf{x}_t$ describes the time-dependent atmospheric state vector; superscript $i = 1, \ldots K$ denotes the i-th forecast experiment ($K = 60$ cases in this study); G symbolizes the dynamical and physical part of the ECMWF model (see next subsection for details); and $\mathbf{F}$ is a *small* and *constant* forcing that is constructed to change the strength of the stratospheric polar vortex in the Northern Hemisphere. The forcing is zero throughout the troposphere. The first set of experiments form the unperturbed control integration (CNTL hereafter); the second and third sets comprise experiments in which the strength of the polar vortex has been increased (STRONG hereafter) and reduced (WEAK hereafter), respectively, by applying the forcing $\mathbf{F}$ during the course of the integration.

For each of the three experiment types (CNTL, STRONG, and WEAK) a total of sixty D+40 forecasts[1] were carried out; the forecasts were started on 1 December, 1 January, and 1 February of each of the winters from 1981/82 to 2000/01. The fact that the initial dates are at least one month apart takes into account the rather persistent character of stratospheric anomalies (Baldwin et al., 2003) and ensures that each of the 60 D+40 forecasts represents an independent realization, thus increasing the confidence of the results.

Throughout the remainder of this section the ECMWF model is described in brevity. Then the sketch of method that has been used to construct the optimal forcing vector **F** is described.

2.1 Model

The model, *G*, used to carry out the nonlinear integrations is one of the latest versions of the ECMWF model (cycle 28r1) that has been used operationally from 9 March to 27 September 2004. In this study a horizontal resolution of T_L95 (linear Gaussian grid, $\approx 1.875^o$) is used and 60 levels in the vertical are employed. About half of the levels are located above the tropopause, that is, the vertical resolution of the stratosphere is relatively high (e.g., Untch and Simmons, 1999). The highest model level is located at about 0.1 hPa. Some aspects of the model performance at this resolution, including the stratosphere, are discussed elsewhere (Jung and Tompkins, 2003; Jung, 2005). In particular the study by Jung and Tompkins (2003) shows that the model climate in the lower and middle stratosphere agrees very well with estimates from the ERA-40 reanalysis.

2.2 Construction of the forcing

The forcing **F**, which is used to change the strength of the stratospheric polar vortex, is constructed using the adjoint technique (e.g., Errico, 1997). A brief overview of the method is given. The reader who interested in more details should consult the references given throughout this section.

Since numerical models are the basic tool of this study in order to investigate the stratosphere-troposphere link, let us start with the prognostic equation employed in numerical weather prediction:

$$d\mathbf{x}/dt = N(\mathbf{x}), \tag{4}$$

where *N* is a non-linear function. Experience from numerical weather forecasting shows that the evolution of **x** is sensitive to small perturbations, both of the initial conditions (e.g.Molteni et al., 1996) and the model tendencies (e.g. Buizza et al., 1999; Barkmeijer et al., 2003). The evolution of sufficiently small perturbations can be described by a linearized version of Eqn. (4), that is,

$$d\delta\mathbf{x}/dt \approx \mathbf{N}_L\delta\mathbf{x} + \mathbf{f}, \tag{5}$$

where $\delta\mathbf{x}$ is a small perturbation of the atmospheric state vector (difference between perturbed and unperturbed forecast); $\mathbf{N}_L$ is the Jacobian of *N*; and **f** represents a small, time-dependent forcing of the model tendencies.

The solution of Eqn. (5) takes the following form (e.g.. Barkmeijer et al., 2003):

$$\delta\mathbf{x}_t = \mathbf{M}(0,t)\delta\mathbf{x}_0 + \int_0^t \mathbf{M}(s,t)\mathbf{f}_s ds, \tag{6}$$

where $\delta\mathbf{x}_0$ denotes a perturbation to the initial conditions; $\delta\mathbf{x}_t$ is the perturbation at final time *t*; and **M** is the tangent forward propagator. In this study only the case of $\delta\mathbf{x}_0 = \mathbf{0}$ (no initial perturbations) and $\mathbf{f}_s = \overline{\mathbf{f}} = const$

[1] As is common practice in the numerical weather prediction community, we shall use the expression D+*n* forecast for a *n*-day forecast.

is considered so that Eqn. (6) reduces to

$$\delta \mathbf{x}_t = \widetilde{\mathbf{M}}\bar{\mathbf{f}}, \tag{7}$$

where $\widetilde{\mathbf{M}} = \int_0^t \mathbf{M}(s,t)ds$. Since in nonlinear systems like Eqn. (4) the operator $\widetilde{\mathbf{M}}$ depends on $\mathbf{x}$, the perturbation growths of a given optimal forcing $\bar{\mathbf{f}}$ is flow-dependent (e.g. Palmer, 1993).

Here, we are interested in such forcing perturbations $\bar{\mathbf{f}}$ that are efficient in changing the strength of the stratospheric polar vortex, that is, at final time t the evolved perturbation $\delta\mathbf{x}_t$ should project strongly onto stratospheric polar vortex anomalies ($\delta\mathbf{x}_{SPV}$, hereafter). In order to quantify the difference between $\delta\mathbf{x}_t$ and $\delta\mathbf{x}_{SPV}$ we use the following cost function:

$$J(\bar{\mathbf{f}}) = \frac{1}{2} < \mathbf{P}(\widetilde{\mathbf{M}}\bar{\mathbf{f}} - \delta\mathbf{x}_{SPV}), \mathbf{C}_F\mathbf{P}(\widetilde{\mathbf{M}}\bar{\mathbf{f}} - \delta\mathbf{x}_{SPV}) > . \tag{8}$$

$\mathbf{P}$ denotes the projection operator (Buizza, 1994), which is used for localization in space; $<,>$ represents the Euclidean inner product; and $\mathbf{C}_F$ induces a norm at final time t. The ultimate aim is to find that $\bar{\mathbf{f}}$, which minimizes the cost function J.

In order to solve the minimization problem we use a second-order quasi-Newton method (Gilbert and Lemarechal, 1989). This requires the knowledge of the gradient of J with respect to the forcing perturbation $\bar{\mathbf{f}}$, which can be obtained as follows (e.g. Oortwijn and Barkmeijer, 1995; Rabier et al., 1996; Barkmeijer et al., 2003, for details):

$$\nabla_{\bar{\mathbf{f}}} J = \mathbf{C}_E^{-1}\widetilde{\mathbf{M}}^T\mathbf{P}^T\mathbf{C}_F\mathbf{P}(\widetilde{\mathbf{M}}\bar{\mathbf{f}} - \delta\mathbf{x}_{SPV}). \tag{9}$$

This gradient—also sometimes refered to as the *sensitivity* (Oortwijn and Barkmeijer, 1995; Rabier et al., 1996)—depends on (i) the pattern being investigated (here, $\delta\mathbf{x}_{SPV}$), the tangent linear propagator $\widetilde{\mathbf{M}}$ and its adjoint $\widetilde{\mathbf{M}}^T$ and, therefore, also the actual flow, (iii) the area being targeted, and (iv)the norms being used at initial and final time ($\mathbf{C}_E$ and $\mathbf{C}_F$, respectively).

In this study, an optimization time of $t = 48$ hours is used. The focus is on the Northern Hemisphere and localization is achived by using the projection operator, which sets all values south of 30°N effectively to zero. Diabatic versions of $\widetilde{\mathbf{M}}$ and $\widetilde{\mathbf{M}}^T$ are used at a horizontal resolution of T63 and with 60 levels in the vertical. The linearized physics are the same as in Mahfouf (1999) comprising vertical diffusion, large-scale condensation, long-wave radiation, deep cumulus convection, and subgrid-scale orographic effects. The minimization of the cost function is based on 6 iterations (see Klinker et al., 1998, for further details).

The total energy norm is used for $\mathbf{C}_E$ and $\mathbf{C}_F$, which is defined as follows:

$$< \mathbf{x}, C_{TE}\mathbf{x} > = \frac{1}{2}\int\int\left[u'^2 + v'^2 + \frac{c_p}{T_r}T'^2 + c_q\frac{L^2}{c_pT_r}q'^2\right]d\Sigma\frac{\partial p_r}{\partial\eta}d\eta + \frac{1}{2}\int\left[R\frac{T_r}{p_r}\ln p_s'^2\right]d\Sigma, \tag{10}$$

where u', v', T', p_s', and q' are perturbations of zonal wind, meridional wind, temperature, surface pressure and humidity, respectively (e.g., Ehrendorfer et al., 1999, for details). The integration is carried out over the whole horizontal domain $\hat{\Sigma}$ and all vertical levels η. In this study $c_q = 0.0$ so that Eqn. (10) reduces to the *dry* total energy norm.

The pattern used to representing stratospheric polar vortex anomalies is based on the full three-dimensional state vector of the NAO, that is, $\delta\mathbf{x}_{SPV} \equiv \delta\mathbf{x}_{NAO}$. Recall that the state vector encompasses vorticity, divergence, temperature, the logarithm of surface pressure and specific humidity on all 60 model levels. In order to contruct this pattern we have made use of ERA-40 reanalysis data (Uppala et al., 2005) truncated at T63 in order to match the resolution used for minimization. First, the NAO index has been constructed for each of the months from December–March of the period 1958–2001 by taking the difference between normalized monthly-mean sea level pressure time series from the Azores and Iceland (Walker, 1924; Hurrell, 1995a). Then high and low

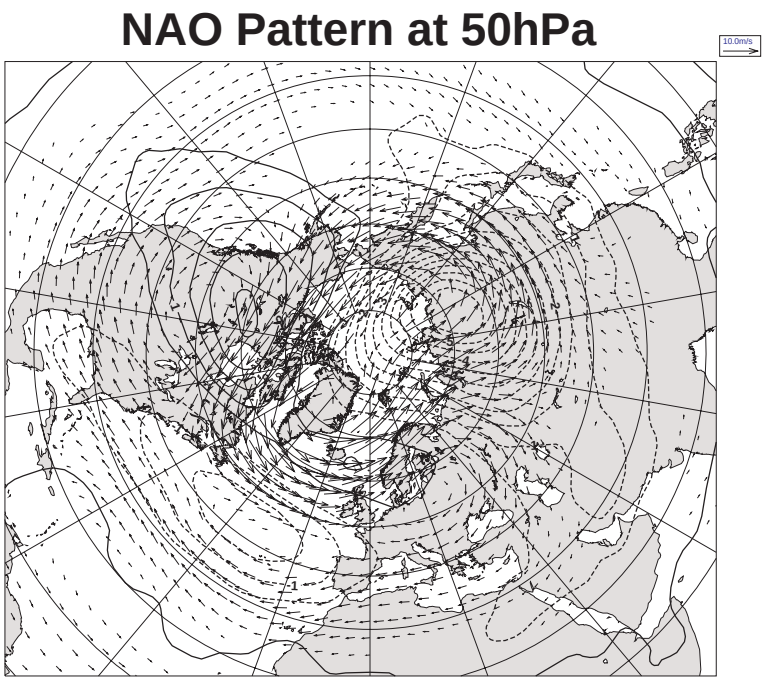

Figure 1: Anomalous wind (ms^{-1}) and temperature (contour interval is 0.5 K) fields at about 50 hPa that are associated with the positive phase of the NAO during wintertime (Dec–Mar). Positive (negative) temperature contours are solid (dashed). Results are based on compositing monthly-mean ERA40 data at model level 22 (about 50 hPa) according to the monthly-mean value of the observed NAO index.

NAO composites have been formed by averaging all monthly-mean state vectors for which the NAO index is one standard deviation above and below normal, respectively. The NAO pattern, $\delta\mathbf{x}_{NAO}$, used during the course of the minimization is the difference between the high and low NAO composites. Both, the NAO index and the three-dimensional state vector is based on ERA-40 reanalysis data (truncated at T63). The NAO pattern in shown Fig. 1 for anomalous horizontal wind vectors and temperatures at about 50 hPa. Evidently, it reflects an anomalously strong and cold polar vortex.

Next, this pattern has been used to construct optimal forcing perturbations, $\bar{\mathbf{f}}$, for 19 days (each 5 days apart) in the winter 2002/03 using the method outlined above. Then, all the 19 optimal forcing patterns have been averaged to obtain the forcing for the nonlinear model, that is, $\mathbf{F} = <\bar{\mathbf{f}}>$, where $<>$ denotes ensemble averaging. The forcing $\mathbf{F}$ has been set to zero below model level 27 (about 150 hPa), in order to restrict the forcing to the stratosphere only. The transition from non-zero to zero forcing has been slightly smoothed to prevent the generation of a spurious potential vorticity forcing in the lower stratosphere. The vertical profile of the resulting temperature forcing averaged over the area 50–140^{o}E and 60–90^{o}N is shown in Fig. 2. The largest temperature forcing, which leads to an *increase* of the stratospheric polar vortex, appears in the lower stratosphere between about 150 to 50 hPa amounting to -1.0 to -1.5 $K day^{-1}$. Moreover, Fig. 2 highlights the fact that the troposphere remains unperturbed.

The wind and temperature forcing at about 50 hPa, which should be efficient in *increasing* the strength of the stratospheric polar vortex is shown in Fig. 3. The first thing to notice is that this pattern is very similar to the NAO pattern used as input to the adjoint (see Fig. 1). There is, however, a shift of about 20^o to the west in the temperature forcing field compared to the temperature anomaly associated with the NAO. The forcing basically accelerates and cools the stratospheric polar vortex. Moreover, it is evident that the forcing magnitude is relatively small amounting to about 2.5 $ms^{-1}day^{-1}$ for wind speed and 2 $K\,day^{-1}$ for temperature.

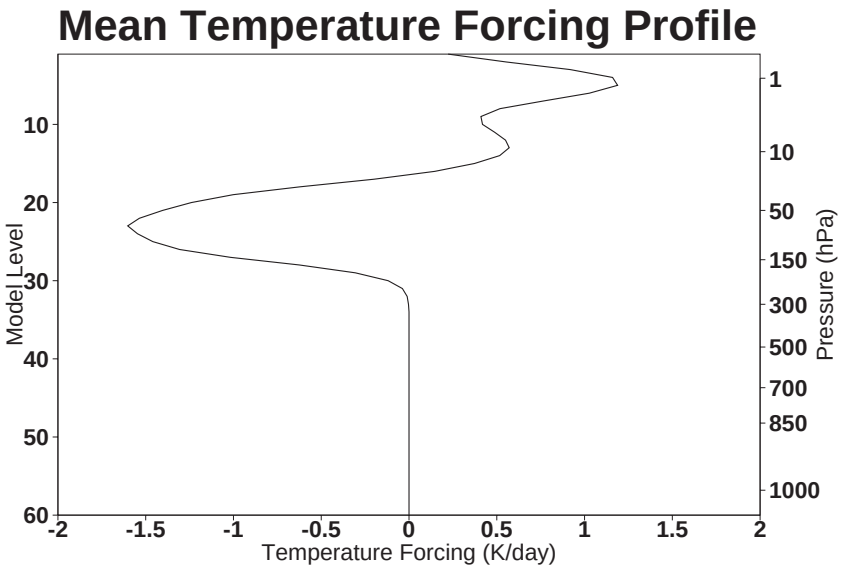

Figure 2: Vertical profile of the mean temperature forcing ($K\,day^{-1}$) averaged over the area 50–140^{o}E and 60–90^{o}N.

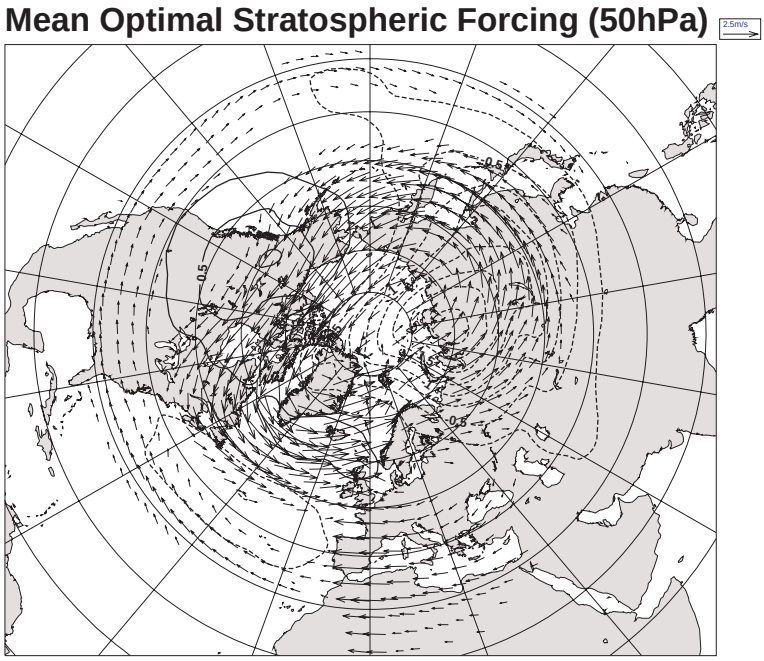

Figure 3: Mean wind ($ms^{-1}day^{-1}$) and temperature (contour interval is 0.25 $K day^{-1}$) forcing at about 50 hPa based on 19 adjoint forcing patterns. This stratospheric forcing is used throughout this study to change the strength of the stratospheric polar vortex. A reference arrow for the wind forcing is also given. Wind forcing vectors with a magnitude below 0.5 $ms^{-1}day^{-1}$ have been omitted. Positive (negative) temperature forcing contours are solid (dashed).

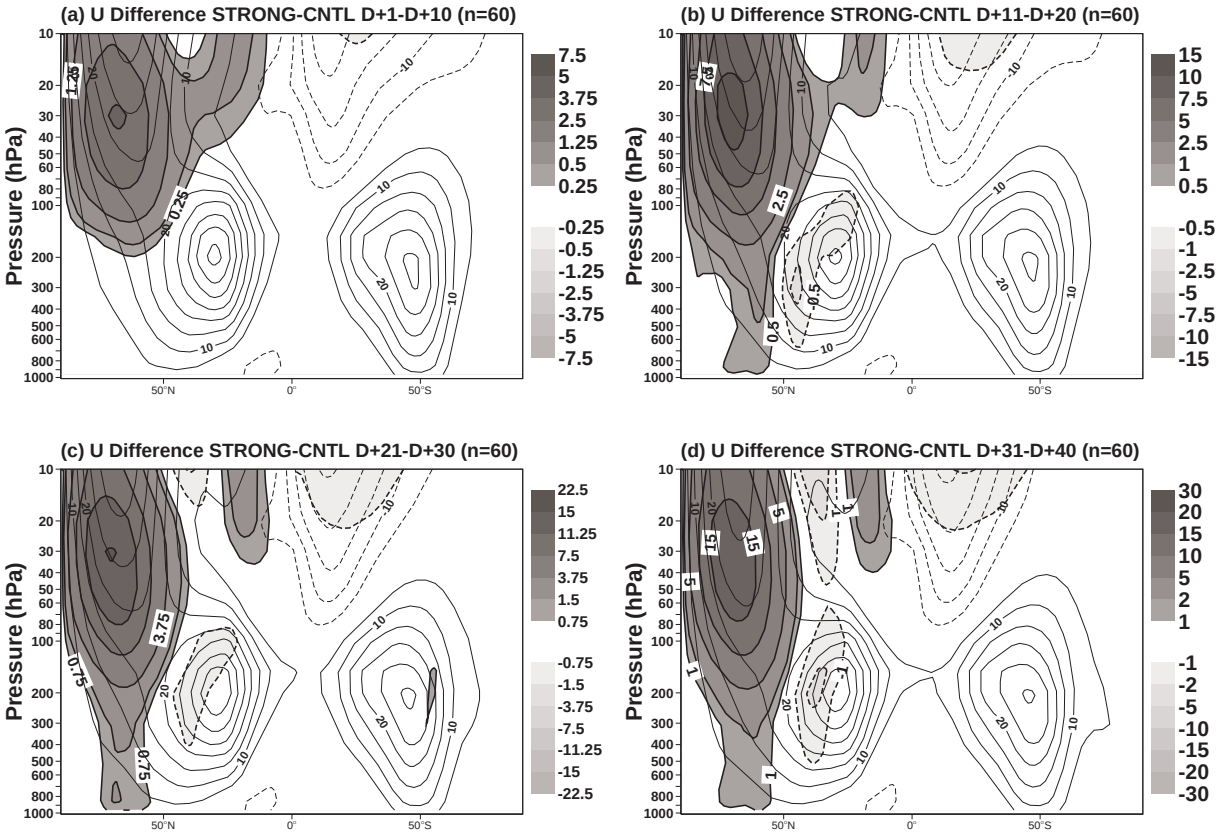

Figure 4: Difference of average zonal-mean zonal winds (shading in ms^{-1}) between the strong polar vortex (STRONG) and the control experiment (CNTL) for 10 day averages: (a) D+1 to D+10, (b), D+11 to D+20, (c) D+21 to D+30 and (d) D+31 to D+40. Shown is the average over 60 different cases (40-day integrations). Notice that the contour interval for the differences changes linearly with the forecast range. Also shown are zonal-mean zonal winds from the control integration (contour interval is 5 ms^{-1}).

3 Results

3.1 Zonal-mean zonal winds

Changes in the strength of the stratospheric polar vortex have a strong zonally symmetric component. Thus, an effective way to evaluate the experiments described in the previous section is to consider zonal-mean zonal winds. The differences of the averaged (over all 60 cases) zonal-mean zonal winds between STRONG and CNTL is shown in (Fig. 4) for three different forecast ranges, that is, for averages from D+1 to D+10, D+11 to D+20, D+21 to D+30 and D+31 to D+40. Also shown are average zonal-mean zonal winds for the control integration CNTL. The first thing to notice is that the forcing **F**, which is based on the adjoint technique, is very efficient in changing the strength of stratospheric polar vortex. The maximum change is found around 30 hPa. Moreover, the perturbation growth (STRONG minus CNTL) is more or less linear in the stratosphere. During the last 10 days of the integration (D+31 to D+40) the polar vortex in STRONG is almost twice as strong as that in CNTL.

Differences of the average zonal-mean zonal wind are also evident in the Northern Hemisphere troposphere, at least after 10 days or so into the integration. These changes encompass an increase of the zonal-mean westerly winds between 50–70^{o}N (polar jet stream) and a decrease of the subtropical jet at its northern flank. In the

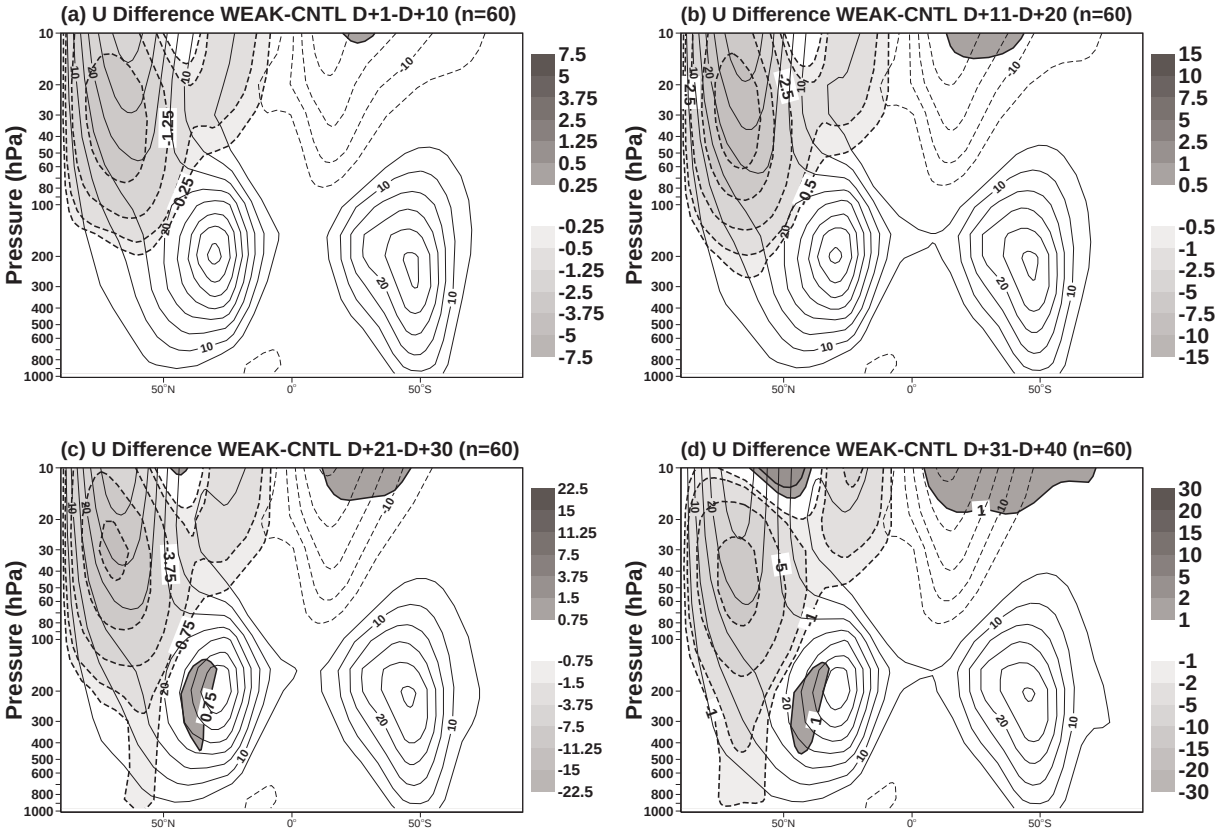

Figure 5: Same as in Fig. 4, except for the difference between experiment WEAK (weak vortex) and CNTL (control).

Northern Hemisphere mid-latitudes the increase of zonal-mean winds in STRONG amounts to about 10–20% of the average zonal-mean winds in CNTL. From the above diagnostics it is evident that, by construction, **F** is very efficient in altering the circulation in the stratosphere. Furthermore, a relatively strong response is found in the Northern Hemisphere troposphere, where the forcing **F** is zero (Fig. 2). This shows that the wintertime tropospheric circulation in the ECMWF model is indeed sensitive to changes in the strength of the stratospheric polar vortex.

The difference of the average zonal-mean zonal winds between WEAK and CNTL is shown in Fig. 5. The strength of polar vortex in the former experiment is clearly weakened compared to the control integration. During the last 10 days of the 40-day integrations the polar vortex has almost completely collapsed at around 50 hPa. Furthermore, it is evident that the difference between WEAK and CNTL is virtually the same as that for the difference between STRONG and CNTL, both in the stratosphere and the troposphere, except for the expected change in the sign of the difference. This resemblence implies that the response to the forcing **F** is to a large degree linear. The main difference between the experiments STRONG and WEAK is that the response for the former is slightly larger.

3.2 Mean Geopotential height fields

After having described the vertical structure of the zonally symmetric response of the ECMWF model to changes in the strength of the polar vortex, in the following the response of the horizontal circulation will be discussed in more detail.

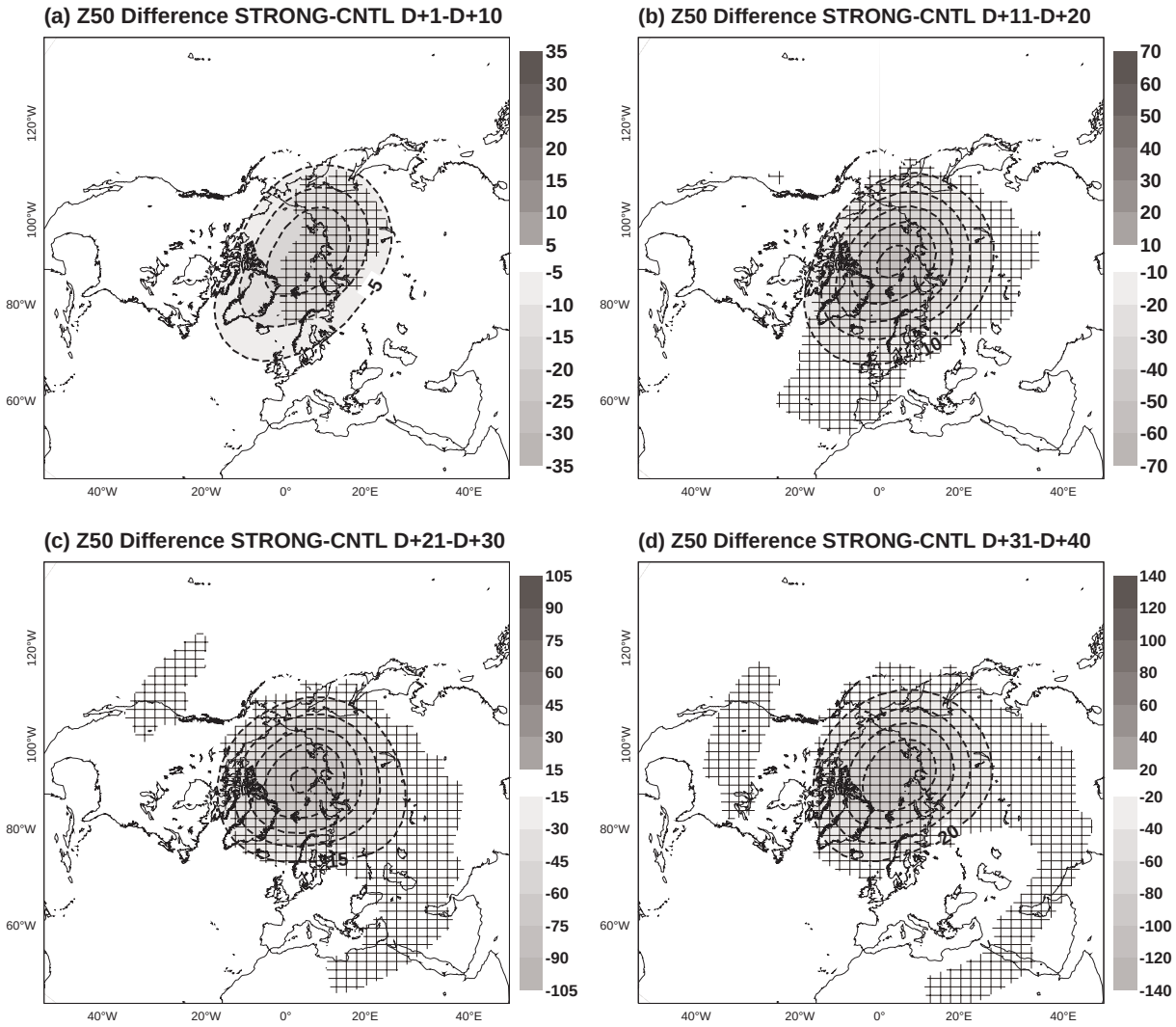

Figure 6: Difference of 50 hPa geopotential height (shading in dam) between the strong polar vortex (STRONG) and the control experiment (CNTL) for 10 day averages: (a) D+1 to D+10, (b), D+11 to D+20, (c) D+21 to D+30 and (d) D+31 to D+40. Shown is the mean over 60 different cases (40-day integrations). Notice that the contour interval for the differences changes linearly with the forecast range. Differences that are statistically significant at the 95% confidence level (two-sided Student's t-test) are hatched.

The difference of mean geopotential height fields at 50 hPa (Z50, hereafter) between STRONG and CNTL is shown in Fig. 6. The forcing **F** leads to a pronounced and statistically significant strengthening of the polar vortex. The evolved perturbation grows at an approximately linear rate throughout the forecast, and during the last 10 days of the integration (D+31 to D+40) Z50 in STRONG is lower by about 800 m over the Arctic compared to CNTL.

The experiment WEAK, with $-\mathbf{F}$ applied to the model tendencies during the integration, shows the same response in Z50, except for a reversal in signs (Fig. 7). The character of the stratospheric response, therefore, appears to be largely linear.

Next, the response of geopotential height fields at 500 hPa (Z500, hereafter) is investigated. The difference of average Z500 between STRONG and WEAK is shown in Fig. 8. Three main centres of action stand out. Anomalously low values of Z500 are found for STRONG in the Greenland/Iceland area, whereas positive

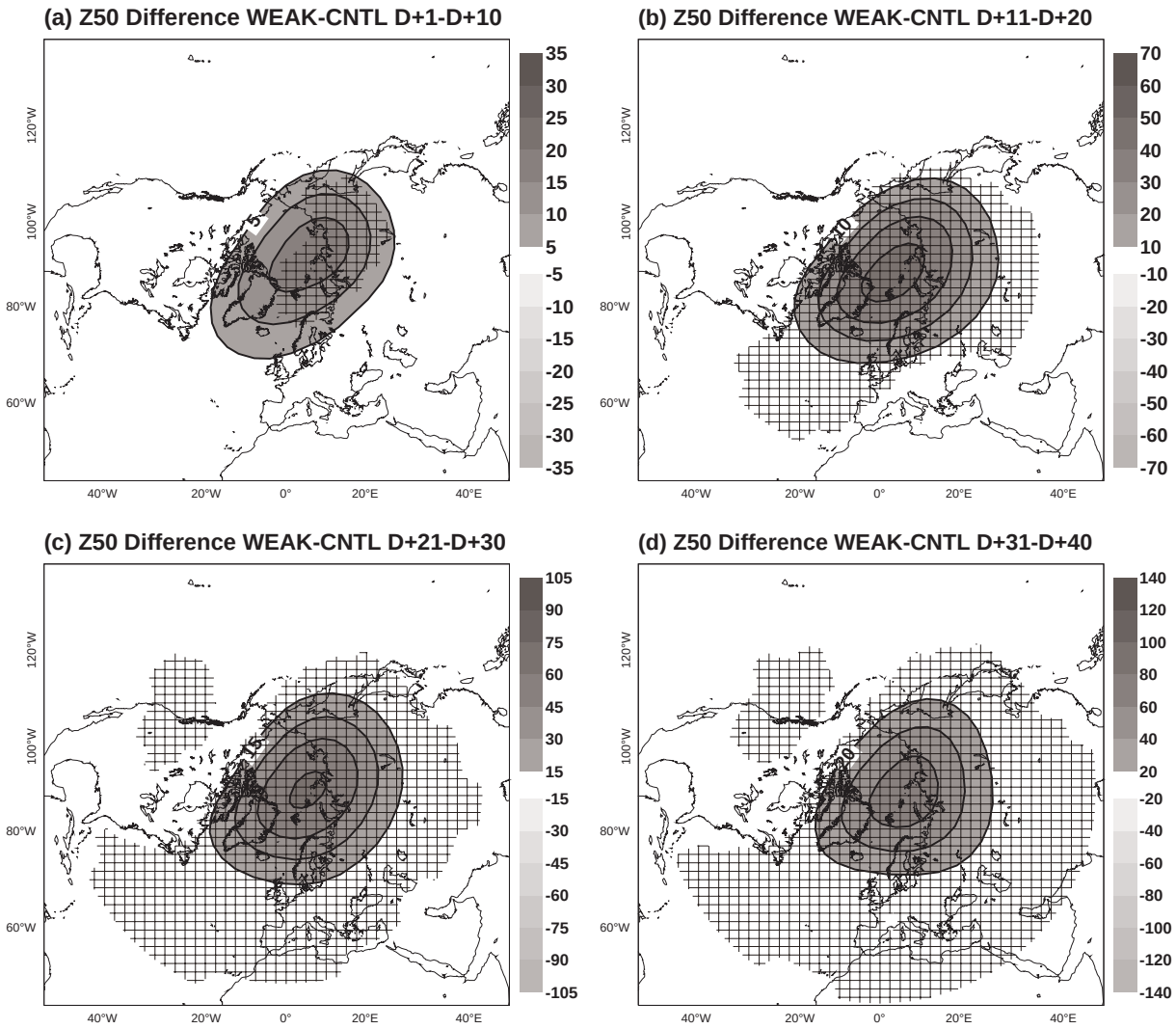

Figure 7: Same as in Fig. 6, except for the difference between experiment WEAK (weak vortex) and CNTL (control).

Z500 differences are evident over Europe and east Asia. No significant response is found in the North Pacific region and over North America. This implies that the response of zonal-mean zonal winds in the mid-latitude troposhere (see Fig. 4) is largely due to zonal wind changes in the North Atlantic region and large parts of Eurasia. The Z500 differences between STRONG and CNTL further show that the perturbation growth is relatively small during the first 10 days or so compared to later forecast ranges (see below). Finally, it is worth mentioning that the Z500 response to a stratospheric forcing shows some resemblance to the NAO, although the Z500 dipole is somewhat shifted to the east compared to the usual pattern of the NAO.

The Z500 difference between WEAK and CNTL (Fig. 9) resembles the response to a strong polar vortex except for a change in sign. This suggests that the tropospheric response at 500 hPa to changes in the strength of the stratospheric polar vortex is largely linear. There are difference in the response between STRONG and WEAK, which to a large degree, however, might be due to sampling variability given that the signal to noise ratio of the tropospheric response is lower than that in the stratosphere (not shown).

The response of the horizontal circulation close to the surface can be infered from Fig.10, which shows the difference of geopotential height fields at the 1000 hPa level (Z500, hereafter) between STRONG and CNTL.

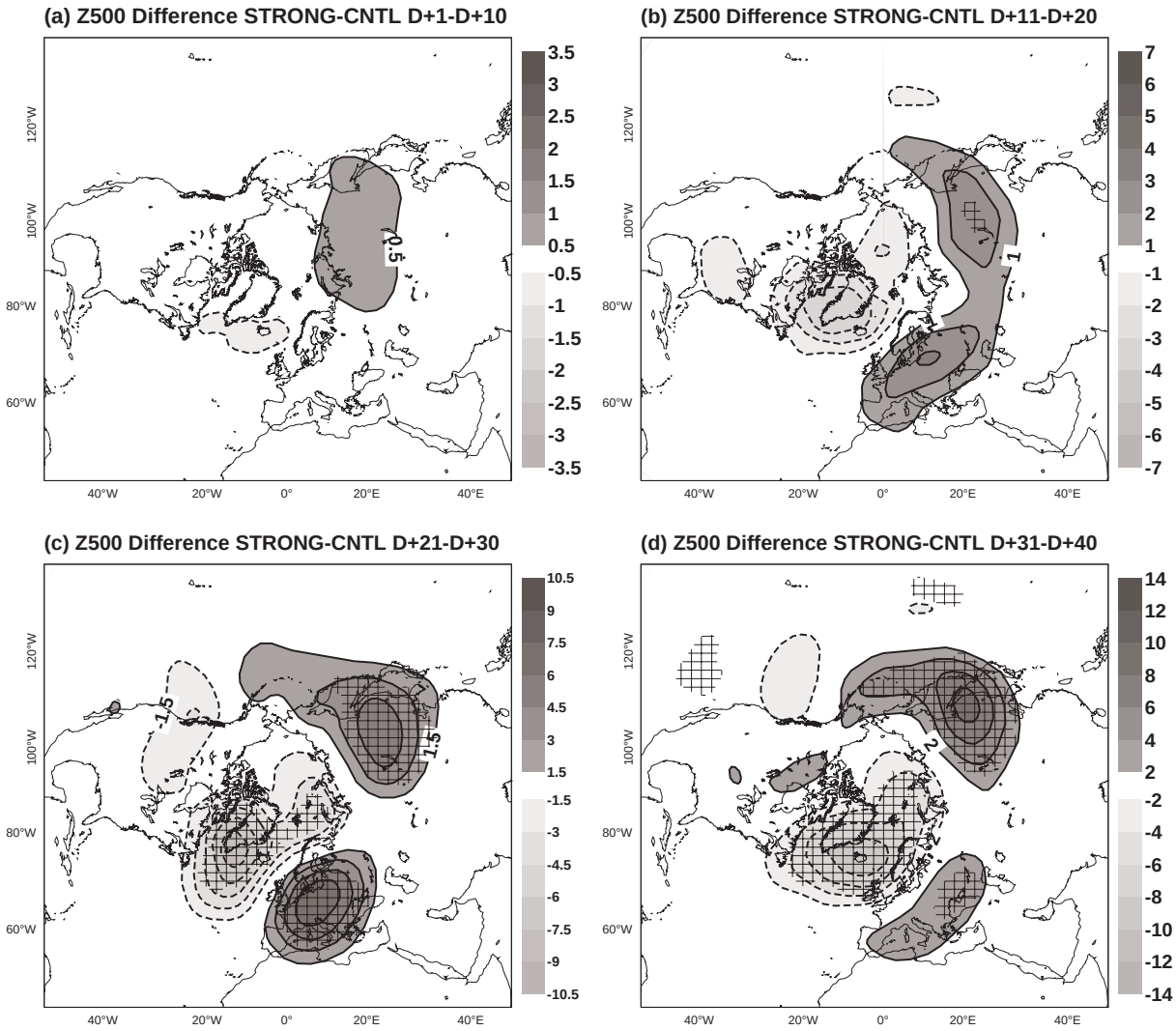

Figure 8: Same as in Fig. 6, except for the 500 hPa level.

Close to the surface, the largest and statistically significant response is found in the north-eastern North Atlantic and parts of the Arctic, at least after more than 20 days into the integration. Interestingly, the strongest initial response occurs in the Greenland/Icelandic area, that is, an area where the NAO has its nothern centre of action.

As for the 50 and 500 hPa level the experiment WEAK shows virtually the same response as STRONG except for a reversal in sign. This suggests that also the near-surface response to changes in the strength of the stratospheric polar vortex is basically linear with respect to the sign of the stratospheric forcing.

As has been briefly mentioned above, there are differences in the rate at which the magnitude of tropospheric perturbations grow during the course of the integration. This result is further substantiated by Fig.12, which shows the evolution of the magnitude of the Northern Hemispheric response, expressed in terms of the Euclidean norm, throughout the forecast at three different vertical levels (50, 500 and 1000 hPa). Note, that results are based on the difference between STRONG and WEAK. Up to D+15 or so, the tropospheric response grows at a lower rate than that in the stratosphere; thereafter the growth in the stratosphere and troposphere is comparable. The exact cause of the delayed tropospheric response is not know. One might speculate, however, that this delay is due to some downward propagtion of the strongest perturbation from the middle to the lower

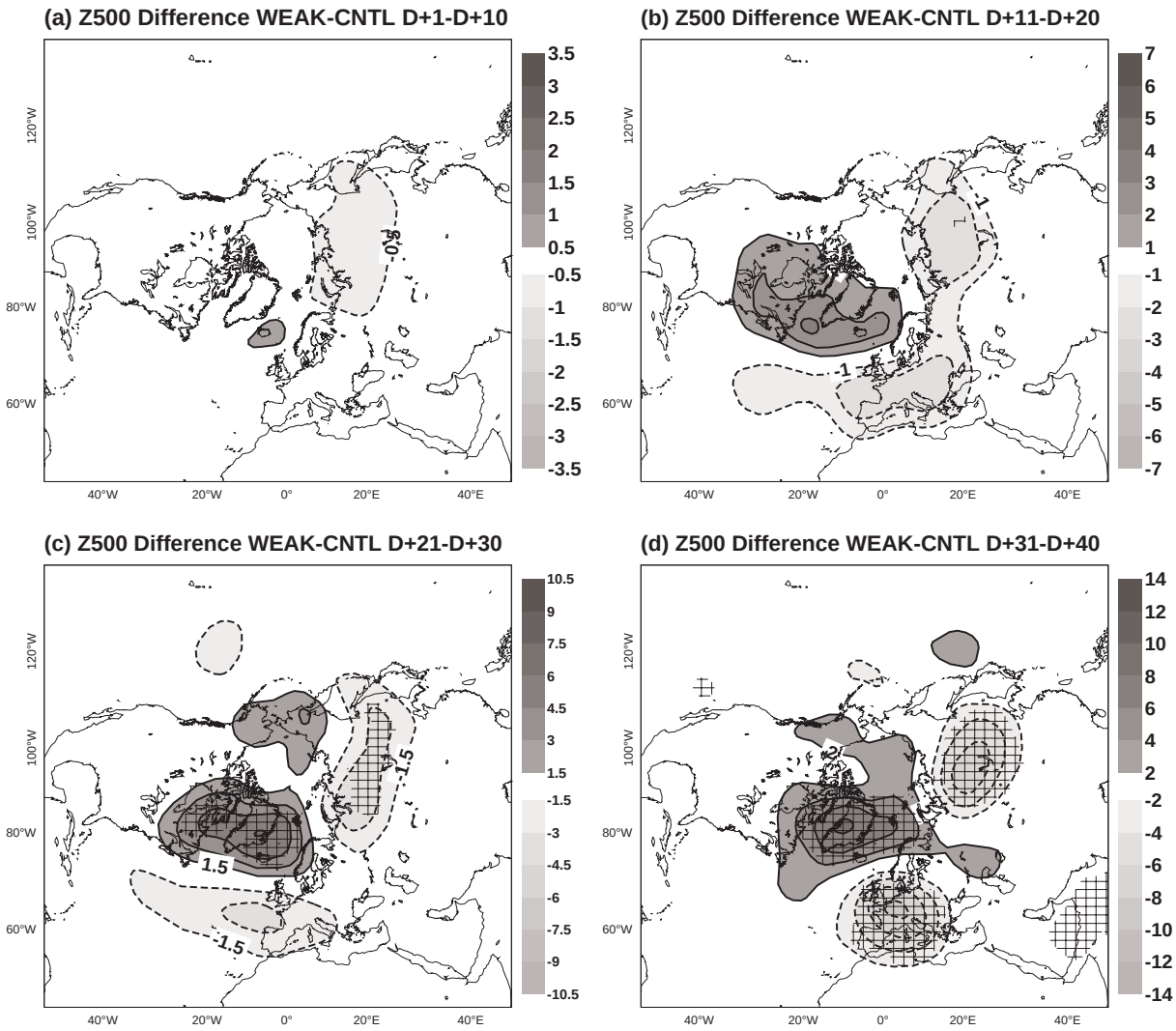

Figure 9: Same as in Fig. 7, except for the 500 hPa level.

stratosphere. Moreover, it is conceivable that non-linear eddy-mean flow interactions in the troposphere are responsible for the delayed accelerated response around D+15 (see below).

3.3 Synoptic-scale transients

The difference of synoptic Z500 activity in the range from D+21 to D+30 between STRONG and WEAK is shown in Fig. 13. Here, synoptic activity is computed by taking the standard deviation of day-to-day Z500 changes. As pointed out by Jung (2005), this filter is particularly useful, if high-pass filtering has to be carried out for short time series (10 day segments in this study). The largest and statistically significant impact of the stratospheric forcing is found over northern Europe and the north-eastern North Atlantic, highlighting the fact that extended-range forecasts for the European region should benefit the most from the stratosphere-troposphere link. Moreover, as shown by Ting and Lau (1993) and Hurrell (1995b) the vorticity fluxes associated with an increased storm track are such to induce a horizontal cyclonic (anti-cyclonic) circulation to its north (south). In this way, the eddies could indeed positively feedback onto the mean large-scale tropospheric anomaly.

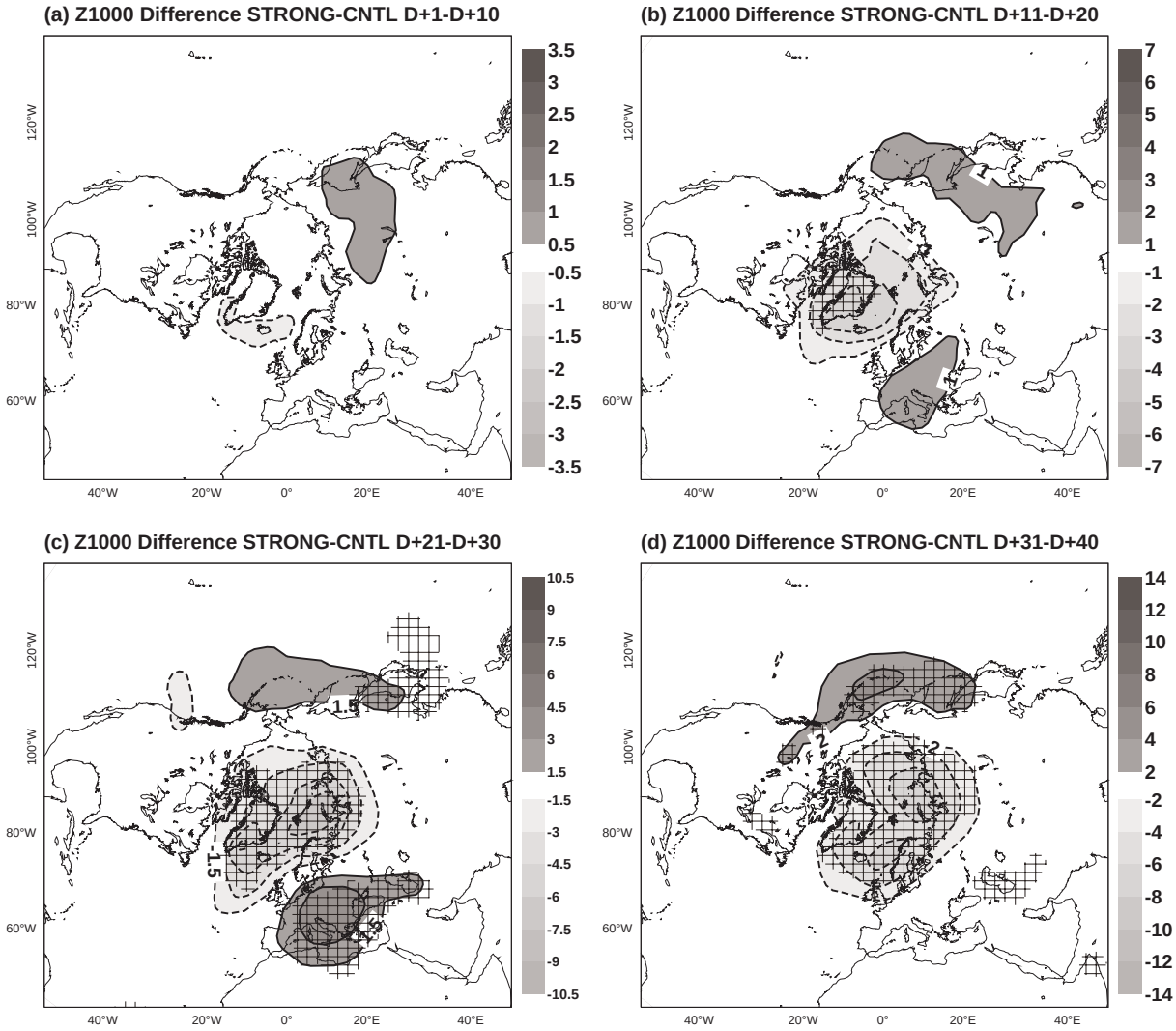

Figure 10: Same as in Fig. 6, except for the 1000 hPa level.

Recently, it has been suggested that the stratospheric influence on the troposphere is in fact mediated by the transient eddies (Charlton et al., 2004; Wittman et al., 2004). This is in contrast to earlier proposed mechanisms of the tropospheric response focussing on large-scale dynamics (e.g. Black, 2002; Ambaum and Hoskins, 2002). In order to help understanding the tropospheric response in the experiments described in this study, average spatial spectra have been computed at D+2, D+4, D+10 and D+20 from Z500 difference fields between STRONG and WEAK (Fig. 14, solid line). Also shown are 95% confidence intervals (using a χ^2-test, shading). At D+2 and D+4 the strongest tropospheric response is found on relatively large spatial scales. This suggests that it is large-scale dynamics, which is crucial during the early stages of the forecast. With increasing lead time the relative importance of synoptic scales becomes more dominant suggesting that for individual perturbed forecasts the mean tropospheric response is considerably masked by superimposed synoptic-scale perturbations.

3.4 Climatology of stratospheric vortex variability

The experiment WEAK shows a strong weakening of the polar vortex as reflected by Z50 anomalies in excess of 700 m beyond D+30 (Fig. 7c,d). The corresponding near-surface response in terms of Z1000 amounts to

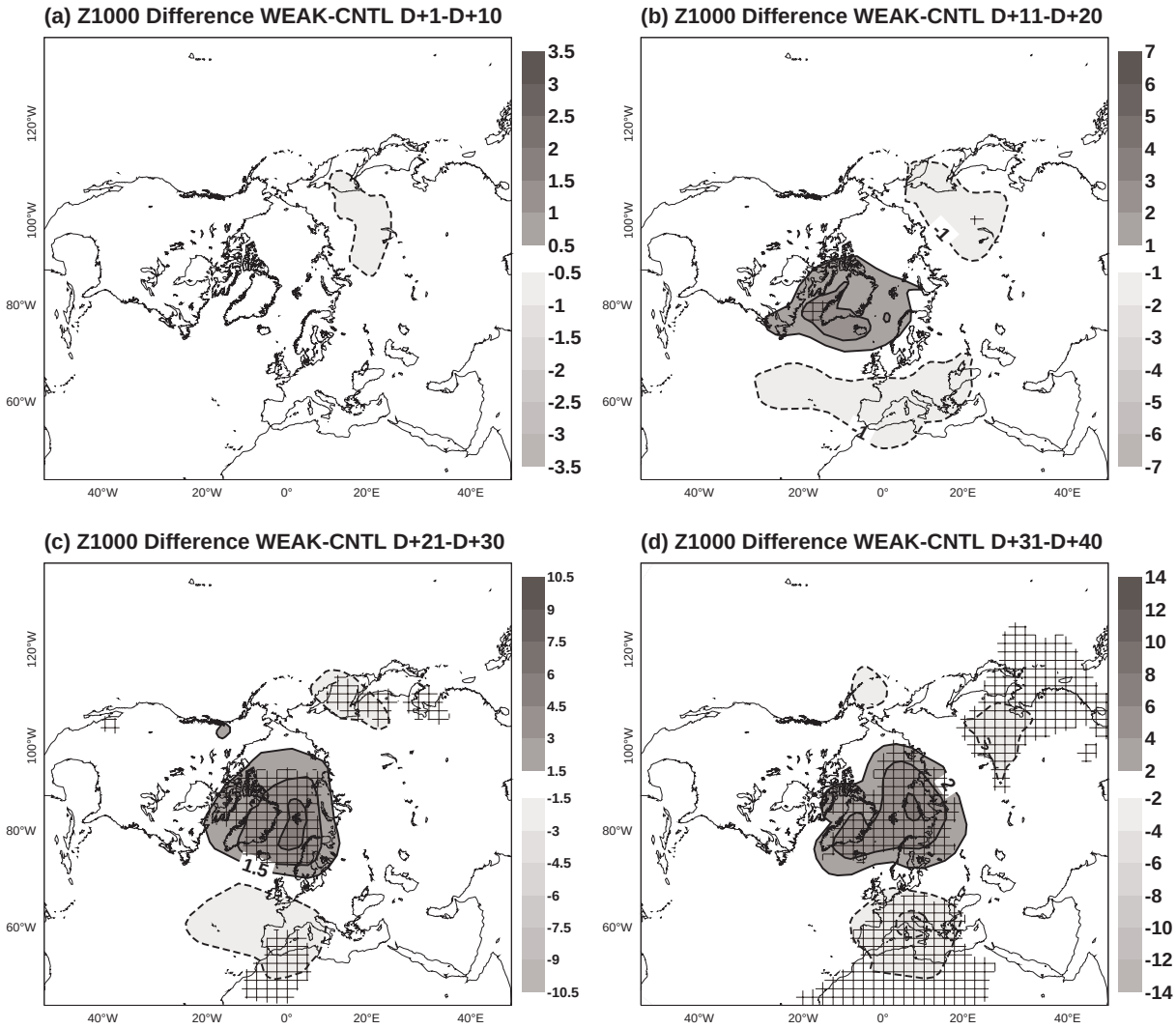

Figure 11: Same as in Fig. 7, except for the 1000 hPa level.

about 60 m (Fig. 7c,d), which is equivalent of a mean-sea level pressure anomaly of about 6 hPa. It is natural to ask, how unusual such anomalies of the stratospheric polar vortex are in nature.

In order to answer this question, empirical orthogonal function (EOF) analysis has been carried out for ten-day averaged Z50 anomalies north of 50°N obtained from the ERA-40 reanalysis (Uppala et al., 2005). Only winters (December through March) of the years 1980–2001 were considered. The average annual Z50 cycle has been removed beforehand. The first EOF, which is shown in Fig. 15, clearly reflects changes in the strength of the polar vortex. It explains 63% of the total Z50 variance in the domain considered. In contrast to the Z50 response in STRONG and WEAK, however, the centre, which shows anomalies of about 350 m, is slightly closer located to Greenland. The corresponding principal component (PC), by construction, is normalized to unit variance, that is, the Z50 anomaly shown in Fig. 15 corresponds to a value of PC=1.0.

The smoothed cumulative probability density function (CDPF) of the first PC is shown in Fig.16. The first thing to notice is that the PC is negatively skewed, which shows that weak polar vortex cases tend to be more extreme than strong ones (see also Monahan et al., 2003). A comparison of the response of WEAK and STRONG beyond D+30 in terms of Z50 (Figs. 6 and 7) with the first EOF of Z50 anomalies (Fig. 15) reveals that the

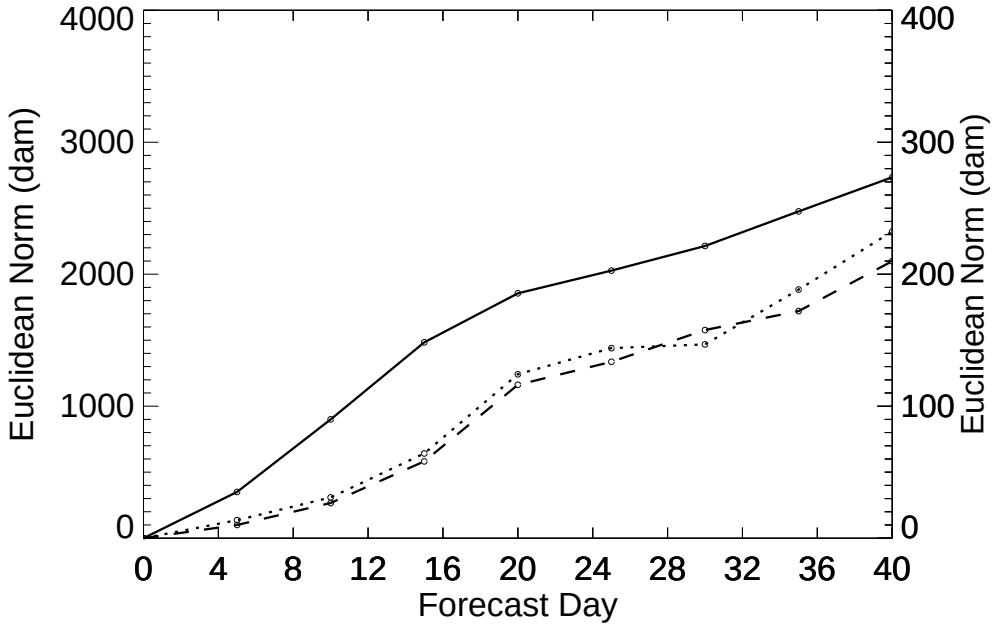

Figure 12: Eucidean norm (dam) of the average geopotential height difference between strong (STRONG) and weak (WEAK) polar vortex cases at 50 hPa (solid), 500 hPa (dotted), and 1000 hPa (dashed) as a function of forecast time (averages from D+1 to D+5, D+6 to D+10 and so forth). Values on the left (right) ordinate refer to stratospheric (tropospheric) levels. Area weighting has been taken into account.

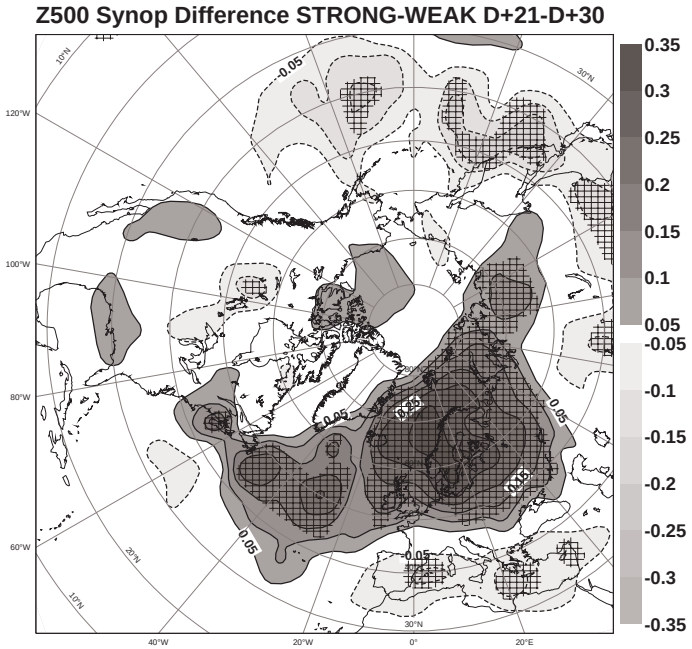

Figure 13: Difference in synoptic activity in the range from D+21 to D+30 ($dam\,day^{-1}$) between STRONG and WEAK. Synoptic actvity is defined as the standard deviation of day-to-day Z500 changes. Statistically significant differences (at the 95% confidence level) are hashed.

former corresponds to values of PC$\pm$2. From the CDPF it can be inferred that these cases are rather extreme, although they do occur—in about 5% and 1% of the ERA-40 anomalies.

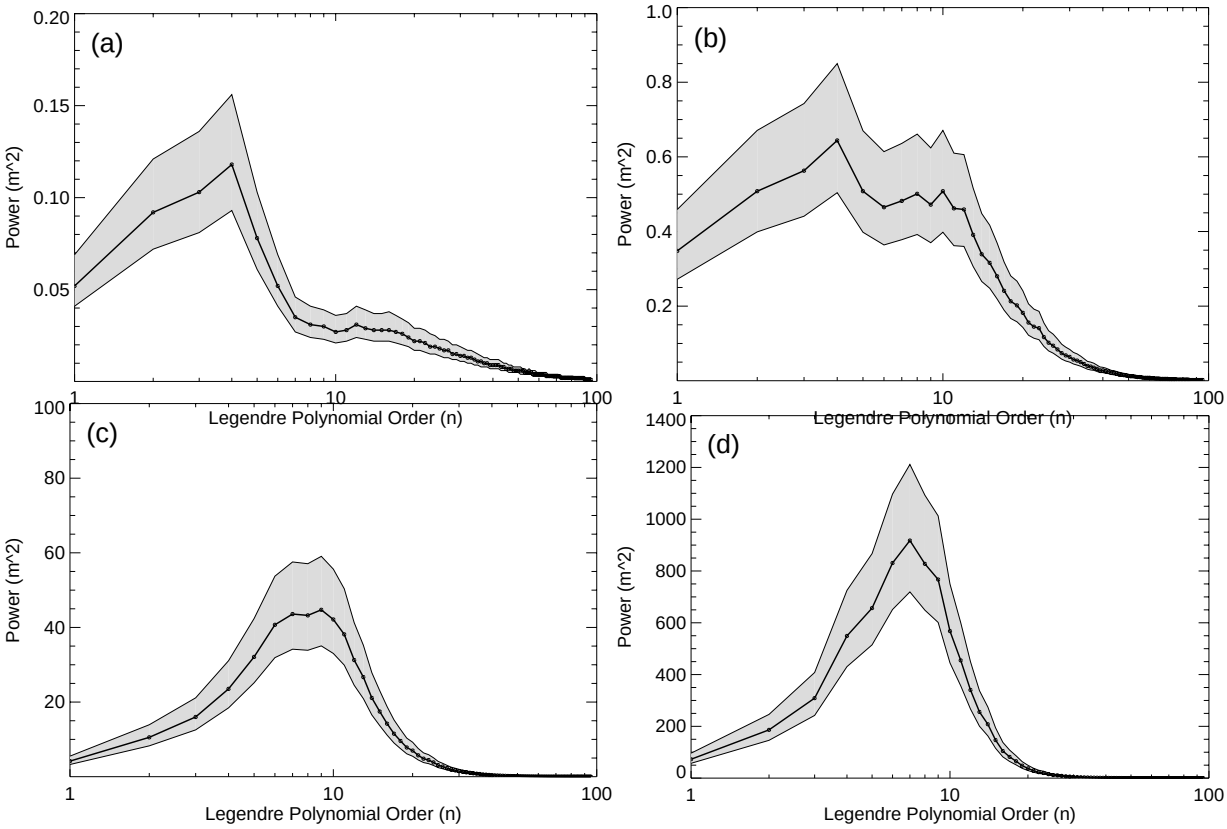

Figure 14: Averaged power spectra (m^2, solid) of the Z1000 difference between STRONG and WEAK as a function of total wavenumber: (a) D+2, (b) D+4, (c) D+10, and (d) D+20. For each forecast step and case (a total of 60 cases were considered), first, the power spectrum of the coefficients of the spherical harmonics has been computed. Then, the resulting 60 spectra have been averaged. Also shown are 95% confidence intervals (shaded area). Notice, that the above diagnostics are global due to the use of spherical harmonics.

4 Discussion

A recent version of the ECMWF model has been used to study the transient response of the tropospheric circulation to changes in the strength of the Northern Hemisphere stratospheric polar vortex. The focus has been on the winter season (December through March). The stratospheric polar vortex has been altered by applying a small forcing to the models vorticity, divergence and temperature tendencies in the stratosphere only, leaving the model dynamics and physics as well as the initial conditions unchanged. The forcing has been obtained using the adjoint technique. In agreement with previous studies (Boville, 1984; Polvani and Kushner, 2002; Black, 2002; Ambaum and Hoskins, 2002; Charlton et al., 2004) a statistically significant response has been found throughout the troposphere, encompassing the mean circulation as well as a change of the storm track. From the transient experiments discussed in this study it is argued that the tropospheric response might be large enough to be of value for extended-range predictions, particularly in Europe.

It would be of practical interest to quantify the skill of dynamical extended-range forecasts resulting from the stratosphere-troposphere connection. We are planning to carry out such a study using hindcasts of the ECMWF monthly forecasting system. Results will be presented in a forthcoming study.

The present study is primarily diagnostic. We think, however, that the results presented allow us to shed light on some aspects of the nature of the stratosphere-troposphere link. Our results imply that it is large-scale dynamics that is responsible for this link, which is consistent with the studies by Black (2002) and

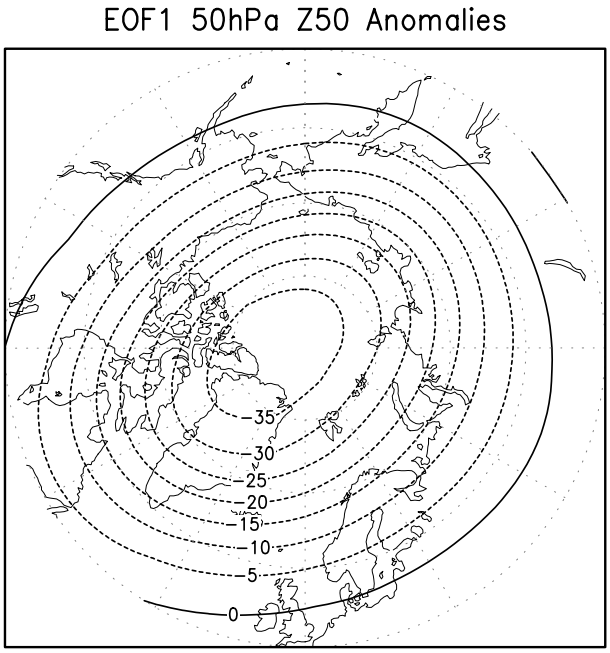

Figure 15: First EOF of 10-day averaged Z50 anomalies (dam) obtained from ERA-40 reanalysis data for all winters (December–March) of the period 1980–2001. The mean annual cycle has been removed prior to EOF analysis. Computations were carried using only data north of 40°N.

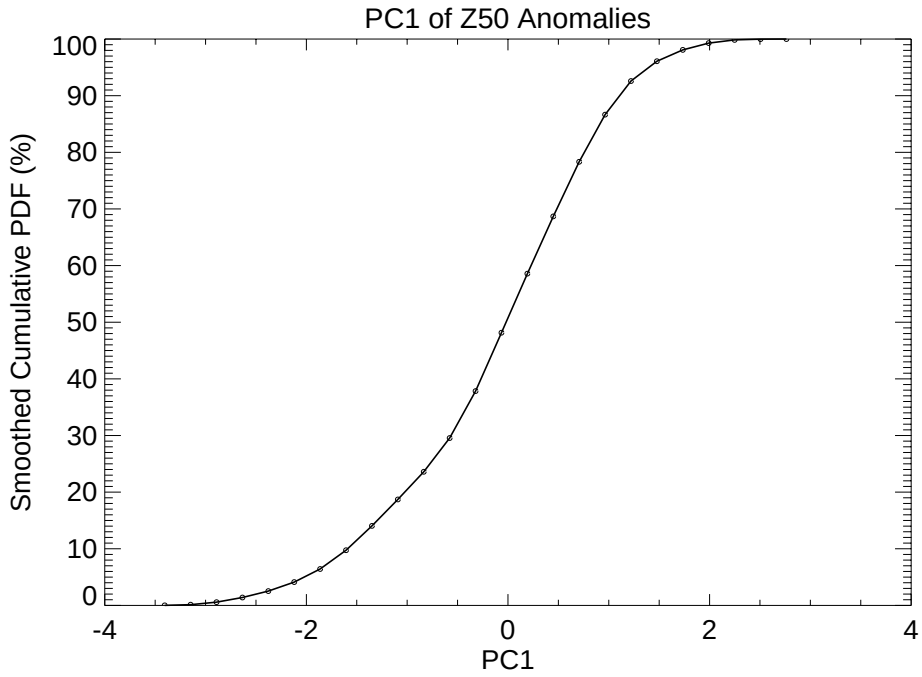

Figure 16: Smoothed cumulative probability density function (CPDF in %) for the first PC of 10-day averaged Z50 anomalies. Smoothing has been carried out using a Gaussian kernel with a window-width of $h = 0.25$ (e.g., Silverman, 1986).

Ambaum and Hoskins (2002). Once, a large-scale tropospheric anomaly is present, perturbations on synoptic scales start to develop, consistent with the notion that growing directions are of small spatial scale (e.g. Toth and Kalnay, 1993; Molteni et al., 1996). The resulting synoptic-scale perturbations are not completely

random; rather there seems to be some organization through the large-scale anomalies. It is likely that the organized synoptic response feeds back positively onto large-scale spatial anomalies, thus, amplifying the tropospheric response to the stratospheric forcing. A very similar role of the transient eddies has been recently proposed by Song and Robinson (2004).

Acknowledgements The authors thank Mark Rodwell for useful discussions. The core of the program used to produce Fig. 14 has been kindly provided by Peter Janssen.

References

Ambaum, M. H. P. and B. J. Hoskins, 2002: The NAO troposphere-stratosphere connection. *J. Climate*, **15**, 1969–1978.

Baldwin, M. P. and T. J. Dunkerton, 2001a: Propagation of the Arctic Oscillation from the stratosphere to the troposphere. *J. Geophys. Res.*, **104**, 30937–30946.

Baldwin, M. P. and T. J. Dunkerton, 2001b: Stratospheric harbingers of anomalous weather regimes. *Science*, **294**, 581–584.

Baldwin, M. P., D. B. Stephenson, D. W. J. Thompson, T. J. Dunkerton, A. J. Charlton, and A. O'Neill, 2003: Stratospheric memory and skill of extended-range weather forecasts. *Science*, **301**, 636–640.

Barkmeijer, J., T. Iversen, and T. N. Palmer, 2003: Forcing singular vectors and other sensitive model structures. *Quart. J. Roy. Meteor. Soc.*, **129**, 2401–2423.

Black, R. X., 2002: Stratospheric forcing of surface climate in the Arctic Oscillation. *J. Climate*, **15**, 268–277.

Boville, B. A., 1984: The influence of the polar night jet in the tropospheric circulation in a GCM. *J. Atmos. Sci.*, **41**, 1132–1142.

Buizza, R., 1994: Localization of optimal perturbations using a projection operator. *Quart. J. Roy. Meteor. Soc.*, **120**, 1647–1682.

Buizza, R., M. Miller, and T. N. Palmer, 1999: Stochastic representation of model uncertainities in the ECWMF Ensemble Prediction System. *Quart. J. Roy. Meteor. Soc.*, **125**, 2887–2908.

Charlton, A. J., A. O. O'Neill, W. A. Lahoz, and A. C. Massacand, 2004: Sensitivity of tropospheric forecasts to stratospheric initial conditions. *Quart. J. Roy. Meteor. Soc.*, **130**, 1771–1792.

Charlton, A. J., A. O. O'Neill, D. B. Stephenson, W. A. Lahoz, and M. P. Baldwin, 2003: Can knowledge of the state of the stratosphere be used to improve statistical forecasts of the troposphere? *Quart. J. Roy. Meteor. Soc.*, **129**, 3205–3225.

Ehrendorfer, M., R. Errico, and K. Raeder, 1999: Singular-vector perturbation growth in a primitive equation model with moist physics. *J. Atmos. Sci.*, **56**, 1627–1648.

Errico, R. M., 1997: What is an adjoint model? *Bull. Amer. Meteor. Soc.*, **78**, 2577–2591.

Gilbert, J. C. and C. Lemarechal, 1989: Some numerical experiments with variable-storage quasi-Newton algorithms. *Mathematical Programming*, **45**, 407–435.

Hurrell, J. W., 1995a: Decadal trends in the North Atlantic Oscillation: Regional temperatures and precipitation. *Science*, **269**, 676–679.

Hurrell, J. W., 1995b: Transistent eddy forcing of the rotational flow during northern winter. *J. Atmos. Sci.*, **52**, 2286–2301.

Jung, T., 2005: Systematic errors of the atmospheric circulation in the ECMWF forecasting system. *Quart. J. Roy. Meteor. Soc.*, **131**, 1045–1073.

Jung, T. and A. M. Tompkins, 2003: Systematic errors in the ECMWF forecasting system. Technical Report 422, ECMWF, Shinfield Park, Reading, Berkshire RG2 9AX, UK.

Klinker, E., F. Rabier, and R. Gelaro, 1998: Estimation of key analysis errors using the adjoint technique. *Quart. J. Roy. Meteor. Soc.*, **124**, 1909–1933.

Kodera, K., M. Chiba, K. Yamazaki, and K. Shibata, 1991: A possible influence of the polar night stratospheric jet on the subtropical tropospheric jet. *J. Met. Soc. Japan*, **69**, 715–720.

Mahfouf, J.-F., 1999: Influence of physical processes on the tangent-linear approximation. *Tellus*, **51 A**, 147–166.

Molteni, F., R. Buizza, T. N. Palmer, and T. Petroliagis, 1996: The ECMWF ensemble prediction system: Methodology and validation. *Quart. J. Roy. Meteor. Soc.*, **122**, 73–119.

Monahan, A. H., J. C. Fyfe, and L. Pandolfo, 2003: The vertical structure of wintertime climate regimes of the Northern Hemisphere extratropical atmosphere. *J. Climate*, **16**, 2005–2021.

Norton, W. A., 2003: Sensitivity of Northern Hemisphere surface climate to simulation of the stratospheric polar vortex. *Geophys. Res. Lett.*, **30**, 10.1029/2003GL016958.

Oortwijn, J. and J. Barkmeijer, 1995: Perturbations that optimally trigger weather regimes. *J. Atmos. Sci.*, **52**, 3932–3944.

Palmer, T. N., 1993: Extended-range atmospheric prediction and the Lorenz model. *Bull. Amer. Meteor. Soc.*, **74**, 49–65.

Polvani, L. M. and P. J. Kushner, 2002: Tropospheric response to stratospheric perturbations in a relatively simple general circulation model. *Geophys. Res. Lett.*, **29**, 10.1029/2001GL014284.

Rabier, F., E. Klinker, P. Courtier, and A. Hollingsworth, 1996: Sensitivity of forecast errors to initial conditions. *Quart. J. Roy. Meteor. Soc.*, **122**, 121–150.

Silverman, B. W., 1986: *Density Estimation for Statistics and Data Analysis*. Chapman & Hall/CRC.

Song, Y. and W. A. Robinson, 2004: Dynamical mechanisms for stratospheric influences on the troposphere. *J. Atmos. Sci.*, **61**, 1711–1725.

Thompson, D. W. J. and J. M. Wallace, 1998: The Arctic Oscillation signature in the wintertime geopotential height and temperature fields. *Geophys. Res. Lett.*, **25**, 1297–1300.

Ting, M. and N.-C. Lau, 1993: A diagnostic and modeling study of the monthly mean wintertime anomalies appearing in a 100-year GCM experiment. *J. Atmos. Sci.*, **50**, 2845–2867.

Toth, Z. and E. Kalnay, 1993: Ensemble forecasting at NMC: The generation of perturbations. *Bull. Amer. Meteor. Soc.*, **74**, 2317–2330.

Untch, A. and A. J. Simmons, 1999: Increased stratospheric resolution. ECMWF Newsletter 82, ECMWF, Shinfield Park, Reading, Berkshire RG2 9AX, UK.

Uppala, S., P. W. Kallberg, A. J. Simmons, U. Andrae, V. Da Costa Bechtold, M. Fiorino, J. K. Gibson, J. Haseler, A. Hernandez, G. A. Kelly, X. Li, K. Onogi, S. Saarinen, N. Sokka, R. P. Allan, E. Andersson, K. Arpe, M. A. Balmaseda, A. C. M. Beljaars, L. van de Berg, J. Bidlot, N. Bormann, S. Caires, F. Chevallier, A. Dethof, M. Dragosavac, M. Fisher, M. Fuentes, S. Hagemann, E. Holm, B. J. Hoskins, L. Isaksen, P. A. E. M. Janssen, R. Jenne, A. P. McNally, J.-F. Mahfouf, J.-J. Morcrette, N. A. Rayner, R. W. Saunders, P. Simon, A. Sterl, K. E. Trenberth, A. Untch, D. Vasiljevic, P. Viterbo, and J. Woollen, 2005: The ERA-40 reanalysis. *Quart. J. Roy. Meteor. Soc.*. Submitted.

Vitart, F., 2004: Monthly forecasting at ECMWF. *Mon. Wea. Rev*, **132**, 2761–2779.

Walker, G. T., 1924: Correlation in seasonal variation of weather, IX. *Mem. Indian. Meteor. Dep.*, **24**(9), 275–332.

Wittman, M. A. H., L. M. Polvani, R. K. Scott, and A. J. Charlton, 2004: Stratospheric influence on baroclinic lifecycles and its connection to the Artic Oscillation. *Geophys. Res. Lett.*, **31**, doi:10.1029/2004GL020503.